Oscillations and translation of a free cylinder in a viscous confined flow

Maria Veronica D'Angelo, Jean-Pierre Hulin, and Harold Auradou

Citation: Phys. Fluids **25**, 014102 (2013); doi: 10.1063/1.4775385
View online: http://dx.doi.org/10.1063/1.4775385
View Table of Contents: http://pof.aip.org/resource/1/PHFLE6/v25/i1
Published by the American Institute of Physics.

PHYSICS OF FLUIDS **25**, 014102 (2013)

Oscillations and translation of a free cylinder in a viscous confined flow

Maria Veronica D'Angelo,[1,2,a)] Jean-Pierre Hulin,[2,b)] and Harold Auradou[2,c)]
[1]*Grupo de Medios Porosos, Facultad de Ingeniería, Paseo Colon 850, 1063, Buenos Aires, Argentina and CONICET, Argentina*
[2]*Univ Pierre et Marie Curie-Paris 6, Univ Paris-Sud, CNRS, F-91405. Lab FAST, Bât 502, Campus Univ, Orsay, F-91405, France*

(Received 14 February 2012; accepted 20 December 2012; published online 22 January 2013)

An oscillatory instability has been observed experimentally on an horizontal cylinder free to move and rotate between two parallel vertical walls of distance H. The vertical motion of the cylinder, its rotation about its axis, and its transverse motion across the gap have been investigated as a function of its diameter D, its density ρ_s, of the mean vertical velocity U of the fluid, and of its viscosity ν. The relevant Reynolds number Re is shown to be based on the cell aperture H and on the relative velocity V_r between the fluid and the cylinder. For a blockage ratio D/H above 0.5 and Re above 20, oscillations of the rolling angle of the cylinder about its axis and of its transverse coordinate in the gap were observed together with periodic variations of the vertical velocity. For a given fluid-cylinder pair, the relative velocity V_r as well as the frequency f and the amplitude of the transverse velocity for these oscillations are nearly independent of the flow velocity U. For given cylinder density and fluid characteristics, f is also nearly independent of the ratio D/H in the range investigated. The oscillations could be observed down to values of Re as low as 30: this is lower than usual values for vortex shedding in confined geometries, which suggests that one might deal with a different instability mechanism. © *2013 American Institute of Physics*. [http://dx.doi.org/10.1063/1.4775385]

I. INTRODUCTION

The influence of confinement on the motion of a cylinder facing a flow is relevant to many applications such as the transport of particles or fibers in slits or the development and localization of biofilms inside pores.[1,2] Many studies have been devoted to this problem but dealt mostly with the determination of the forces on the cylinders (for instance, when they are left free to rotate or eccentered in a stationary flow).

In the studies of the hydrodynamical transport of confined cylinders,[3–6] it has usually been assumed that, in the absence of vortex shedding, the motion of the cylinder is steady: the cylinder translates at a constant velocity and, in some cases, rotates at a constant angular velocity and at a fixed transverse distance from the mid plane of the gap. Following these views, non-stationary flows would only appear at Reynolds numbers, Re, above the vortex shedding threshold. The present work reports instead, at Reynolds numbers as low as 30, a periodic non-stationary transport regime, which might reflect another type of flow instability strongly influenced by the viscosity.

Early studies of the torque and drag forces on a cylinder facing a flow have been performed in the Stokes regime or at relatively small Reynolds numbers. For particles placed in the centre of the channel, Faxen[7] derived the expression of the drag for a confinement D/H less then 0.5; the case of higher confinements has been recently considered by Ben Richou and co-workers.[8,9] An eccentered

[a)]Electronic mail: vdangelo@fi.uba.ar.
[b)]Electronic mail: hulin@fast.u-psud.fr.
[c)]Electronic mail: auradou@fast.u-psud.fr.

cylinder experiences, in addition, a positive torque decreasing sharply in the vicinity of the walls;[3–6] for a cylinder translating closely along a wall or held fixed in a Poiseuille flow, this torque tends to generate a rotation of sign opposite to that of contact rolling. This results from the backflow near the second wall and has a sizable influence on the force distribution on the cylinder.[10]

The displacement of a free cylinder released from an eccentric position inside a vertical gap has been computed by Hu[6] for three values of the Reynolds number *Re* based on the terminal velocity and the diameter of the particle. For $Re \leq 5$, the cylinder reaches a final stable transverse position in the middle of the gap. For $Re \simeq 100$, instead, an off-axis cylinder rotates in the direction opposite to the previous one, resulting in a lift force oriented away from the axis: this was accounted for by the appearance of a recirculation zone.[11] However, as the cylinder approaches one of the walls, the recirculation zone recedes because of the interaction between the wake and the wall boundary layer. The rotation and the lift force then change sign again, so that a stable off-axis position is finally found.

Such observations are made at a Reynolds number close to the periodic vortex shedding regime,[12] and are consistent with the conclusions of Zovatto and Pedrizzetti[13] for a non rotating cylinder. Above the critical Reynolds number, vortex shedding may induce vibrations with a frequency and amplitude depending on the mechanical properties of the system.[14–16]

More recently, Semin *et al.*[17] observed that a tethered cylinder placed in a Poiseuille flow between vertical parallel planes oscillates spontaneously at Reynolds numbers well below the threshold for vortex shedding: unlike in the present case, both the vertical and rolling motions of the cylinder were blocked.

The present work deals with an horizontal cylinder free to translate and rotate inside the gap of a vertical Hele Shaw cell. Either this cylinder sediments in a stationary fluid, or is submitted to a vertical Poiseuille flow (i.e., transverse to its axis). The transverse and vertical components of the motion of the cylinder and its rotation about its axis are studied: the influence of physical parameters such as the diameter and density of the cylinder and the viscosity of the fluid and of hydrodynamical variables such as the flow velocity is particularly investigated.

II. EXPERIMENTAL SETUP AND PROCEDURE

The experimental setup consists of a Hele Shaw cell placed vertically (Fig. 1). Its height, width, and aperture are, respectively, $L = 350$, $W = 100$, and $H = 3$ mm. The Hele Shaw cell is obtained by milling two PMMA (plexiglass) plates; using this technique, the local aperture varies by less than 0.1 mm over the cell. The vertical sections of the cell have a Y-shape in their upper part; the upper end of the cell is at the bottom of a rectangular bath with a slit allowing for the flow of the fluid and the insertion of the cylinders. An upward flow may be imposed by a gear pump: the mean fluid velocity *U* is counted in this case as negative.

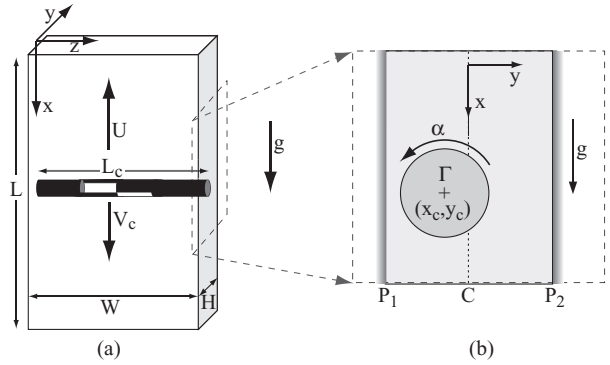

FIG. 1. Experimental setup. (a) Front view - *U*: mean flow velocity, V_{cx}: vertical component of the cylinder velocity. (b) Side view - y_c: transverse position of the center of mass of the cylinder, Γ : Torque.

TABLE I. Physical properties of the fluids. Density: ρ_f, dynamical viscosity: μ. Temperature 23°C. $N1$ and $N2$ correspond to natrosol solutions at, respectively, 1 and 2 g1^{-1}. WG refers to a glycerol solution containing 20% in weight of glycerol.

Fluids	ρ_f (g/cm^3)	μ (mPa s)
WG	1.05	1.56
$N1$	0.998	1.11 ± 0.04
$N2$	0.998	2.20 ± 0.04

In this set-up, at the highest Reynolds numbers $Re_U = UH/\nu \simeq 60$ used here, the entry length for achieving a stationary parabolic flow velocity profile $L \simeq 0.06\, Re_U H$ is of the order of 10 mm: this is much lower than the distance between the inlet and the cylinder (100 − 300 mm). Moreover, an injector is fitted to the bottom part of the cell in order to distribute evenly the flow across the width W of the model. A $2D$ parabolic profile is therefore well established right upstream of the cylinder.

Table I lists the characteristics of the fluids used in the experiments; the viscosity is measured using a Contraves Low Shear-30 rheometer. In this study, the natrosol concentration is sufficiently low so that the fluids can be considered as Newtonian: at a given temperature, their viscosity is determined by the natrosol concentration (and increases with it). For shear rates ranging from 0.2 to 118 s^{-1}, the viscosity (see Table I) of the two natrosol solutions is indeed found to be constant (within ±0.04 mPa s). The density and temperature of the solutions are measured prior to any set of experiments.

The cylinders are made of PMMA (density $\rho_s = 1.20 \pm 0.05$ g cm^{-3}) or of carbon ($\rho_s = 1.54 \pm 0.07$ g cm^{-3}); their mean diameter D ranges from 1.1 to 2.1 mm. The diameter D of the cylinder was measured at five different locations along its length; the value of D was found to vary by less than 0.05 mm. The length L_c of the cylinders is smaller than but as close as possible to the internal width W of the cell.

Initially, the cylinders are placed in the upper bath with their principal axis horizontal and one lets them move down into the Y-shaped zone by reducing the flow rate Q. Then, Q may be adjusted so that the cylinder remains at a fixed mean level either at rest (state 0) or oscillating about its principal axis (state 1). Then, one may reduce Q (sometimes to zero) in order to analyze the motion of falling cylinders; in a part of the experiments, Q is increased again after the cylinder has reached the bottom of the cell for studying its upward motion ($V_{cx} < 0$).

The displacement of the cylinder is monitored by two cameras triggered synchronously at a frame rate of 45 fps; they image, respectively, the displacements in the plane (x, z) over a window of 287×139 mm^2 with a resolution of 0.28 mm/pixel and in the plane (x, y) of the gap with a resolution of 0.111 mm/pixel over a vertical length of 80 mm. Processing digitally the two sets of images gives, first, the instantaneous coordinates (x_c, y_c, z_c) of the center of mass of the cylinder in the (x, z) and (x, y) planes ($y_c = 0$ is in the midplane between the walls). The angle θ between its axis and the horizontal is also determined from the instantaneous location of its two ends in the (x, z) plane. In order to analyze the rotations of the cylinder around its axis, its length is divided into four domains of equal size. The two outside parts are painted in black and two black staggered stripes parallel to the axis are painted on the central portions. The rotation angle α about the axis is estimated from the local vertical distance between each of the stripes and the principal axis of the rod: dividing this distance by the radius of the cylinder gives an estimated value α_{est} of α. The variation of α_{est} with time provides an order of magnitude of the angular velocity $\dot{\alpha}$. These estimations are more valid when the stripe is close to an horizontal diametral plane of the cylinder.

III. DYNAMICAL REGIMES AND TIME AVERAGED CHARACTERISTICS OF CYLINDER MOTION

A. Oscillating and stationary regimes

Figures 2(a)–2(c) display experimental results obtained using a PMMA cylinder of diameter D = 1.1 mm and solution $N1$. In these experiments, the cylinder remains located midway between the

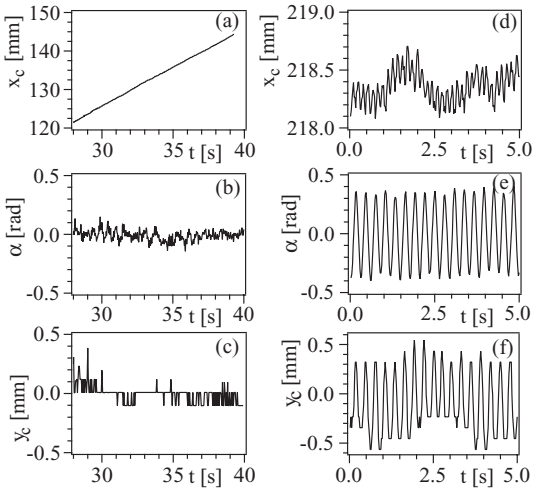

FIG. 2. Experimental measurements obtained using solution $N1$ (see Table I) with left: $D = 1.1$ mm ($D/H = 0.37$) and $U = -16.88\,\mathrm{mm\,s^{-1}}$ and right: $D = 1.77$ mm ($D/H = 0.59$) and $U = -12.66\,\mathrm{mm\,s^{-1}}$. (a) x_c vs time t (s). (b) α vs t. (c) y_c vs t.

two vertical walls ($y_c \simeq 0$ in Fig. 2(c)); it does not roll about its principal axis ($\alpha \simeq 0$ in Fig. 2(b)) and falls at a constant velocity (a linear regression gives $V_{cx} = 2.7 \pm 0.5\,\mathrm{mm\,s^{-1}}$).

Figures 2(d)–2(f) display experimental results obtained using a cylinder with a larger diameter $D = 1.77$ mm. In this case, both the angle α of the cylinder about its axis and its transverse coordinate y_c in the gap oscillate at a well-defined frequency. The mean flow velocity has been selected so that the average of the vertical velocity V_{cx} is zero: the average of the coordinate x_c remains therefore constant but x_c is observed to oscillate with time at exactly twice the frequency observed for α and y_c. In our experiments, this oscillatory regime was only observed for a confinement parameter $D/H \geq 0.48$. The two flow regimes of Figure 2 and the development of these oscillations are discussed in more detail below in Secs. III and IV.

More quantitatively, the period $T_{osc} = 1/f$ of the oscillations has been determined by computing the time interval between the maxima of the first and last oscillations visible in the recording and dividing by the total number N of these oscillations ($15 \leq N \leq 30$). Since this time interval can be determined to within about $T_{osc}/2$, this leads to a relative error on the determination of the frequency of the oscillation: $\Delta f/f = \Delta T_{osc}/T_{osc} \simeq 1/(2N)$: it varies therefore between 1.5% and 3%.

These experiments may be compared to the widely studied situation of a fixed cylinder in a Poiseuille flow. For instance, the numerical simulations of Sahin and Owens,[12] also for a cylinder between parallel plates, suggest that vortex shedding only occurs at Reynolds numbers Re_D above 120 for the same ratio D/H as in Figures 2(d)–2(f) (the definition $Re_D = U_0 D/\nu$ used by these authors is based on the maximum fluid velocity U_0 and the cylinder diameter D). Using this same definition of Re_D, the oscillations displayed in Figures 2(d)–2(f) correspond to a Reynolds number $Re_D \simeq 30$ well below the critical value for vortex shedding mentioned above.

B. Variation of mean vertical translation velocity with the flow velocity

In this section, we are interested in the value of the vertical velocity V_{cx} of the cylinder, averaged over a time larger than the period of the oscillations (if present) but short enough to avoid the influence of global variations. Here, "velocity" always refers to such an average.

Figure 3 displays the variation of V_{cx} with U for the different cylinders and fluids used in the experiments. This variation is found to be linear in all cases for both the oscillating and the stationary regimes. For a same cylinder diameter ($D = 1.45$ mm) and a same fluid ($N1$), the velocity V_{cx} in the oscillating regime is larger at a same velocity U than in the stationary one ((△) and (▲) symbols in Fig. 3). This reflects the lower drag in the stationary regime. Also, the slope of the variation of V_{cx} with U is lower in this latter regime.

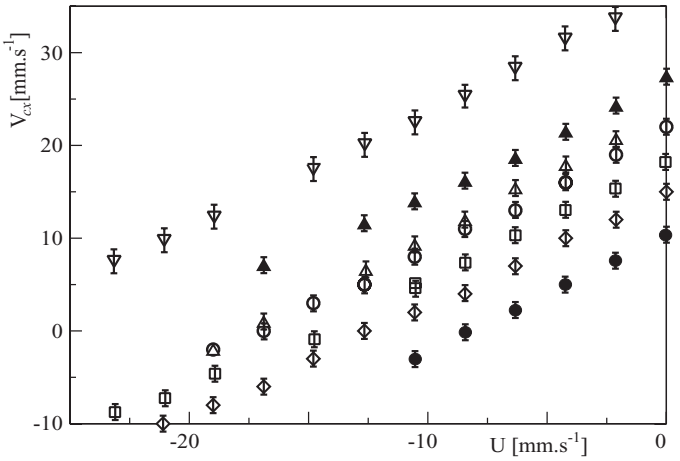

FIG. 3. Vertical velocity V_{cx} of cylinders of diameter D in solutions $N1$ or $N2$ (see Table I) as a function of the fluid velocity U. Open symbols: oscillating cylinders; solid symbols: no oscillations. PMMA cylinders ($\rho_s = 1.20\,\mathrm{g\,cm^{-3}}$) - (△), (▲): $D = 1.45$ mm ($D/H = 0.48$), $N1$; (○), (●): $D = 1.63$ mm ($D/H = 0.54$), $N1$ for (○) and $N2$ for (●); (□): $D = 1.77$ mm ($D/H = 0.59$), $N1$; (◇): $D = 2.1$ mm ($D/H = 0.7$), $N1$. Carbon cylinder ($\rho_s = 1.54\,\mathrm{g\,cm^{-3}}$) - (▽): $D = 1.45$ mm ($D/H = 0.48$), $N2$.

As previously observed by Dvinsky and Popel,[3] the sedimentation velocity V_{cx}^0 in a stationary fluid ($U = 0$) decreases with the confinement: more generally, at a same velocity U, the cylinder velocity V_{cx} is always slightly lower for $D/H = 0.59$ than for $D/H = 0.48$ and significantly lower for $D/H = 0.7$ (respectively, (□), (△), and (◇) symbols in Fig. 3). This result is in agreement with the numerical simulations of Ben Richou *et al.*,[9] still in the confined case: these authors found numerically in the lubrication approximation that the geometrical factor λ_s increases like $D^{5/2}$ for $D/H > 0.1$. Combining the variations of m and λ_s in Eq. (4) (see Sec. III C), the velocity V_{cx}^0 must, then, decrease with D (or equivalently with D/H) as is indeed observed.

An opposite result would be obtained in the low confinement case of cylinders falling in a tank of size much larger than their diameter ($D/H \ll 1$): in that latter case, the sedimentation velocity increases instead with D because the mass m per unit of length varies faster (as D^2) than the drag force.

The experiments also confirm that increasing the fluid viscosity for a same cylinder reduces the value of V_{cx} and results in a transition from an oscillating to a stationary regime ((○) and (●) symbols in Fig. 3). For a significantly larger cylinder density, V_{cx} increases strongly, even for more viscous fluids ((▽) symbols in Fig. 3).

C. Relations between force and flow/cylinder velocities

The value of the vertical velocity V_{cx} reflects an equilibrium between gravity and the vertical drag force F_x (averaged over the same time lapse):

$$mg + F_x = 0; \tag{1}$$

here, $m = \pi\,\Delta\rho\,(D/2)^2$ is the mass per unit length reduced from the effect of buoyancy (with $\Delta\rho = \rho_s - \rho_f$). Since mg is a constant, this implies that the drag force F_x must remain the same, irrespective of the mean flow velocity U. For a cylinder moving at a constant velocity V_{cx} in a fluid of constant mean velocity U away from the cylinder, the drag may be written in the low Reynolds number limit and when the cylinder does not rotate:

$$F_x = -\lambda_s\,\mu\,V_{cx} + \lambda_p\,\mu\,U = -mg. \tag{2}$$

The parameters λ_s and λ_p reflect the influence of the geometrical confinement and of the flow profiles which are different for the flows associated to V_{cx} and U. For a long cylinder ($L_c \simeq W \gg D$ and $L_c \gg H$), λ_s and λ_p are only functions of the ratio of the cylinder diameter D and of the cell aperture

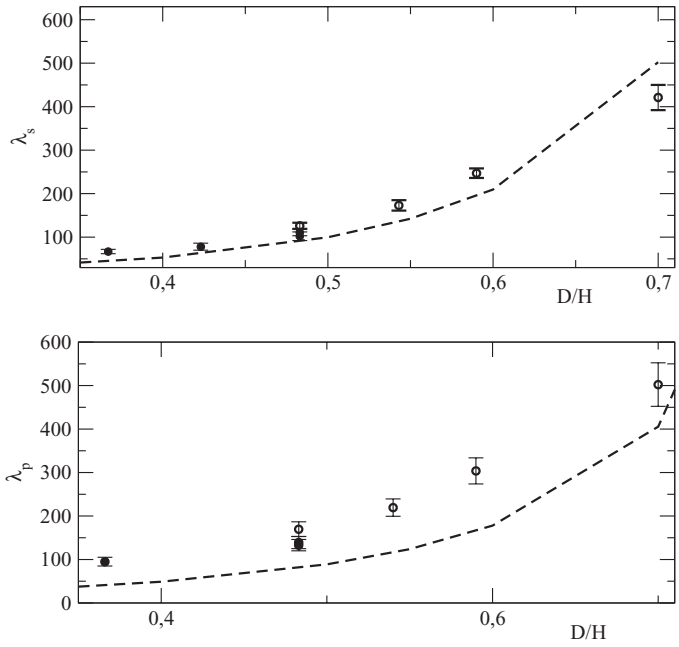

FIG. 4. Top: Variations of λ_s (top) and λ_p (bottom) vs D/H. (○), (●): experimental values of λ_s (top) and λ_p, respectively, with and without oscillations; dashed lines: numerical data from Ref. 9 (for λ_s) and Ref. 8 (for λ_p).

H.[18] The vertical velocity of the cylinder is then

$$V_{cx} = \frac{\lambda_p}{\lambda_s} U + V_{cx}^0, \tag{3}$$

in which

$$V_{cx}^0 = mg/(\lambda_s \mu) \tag{4}$$

is the velocity of the cylinder with no applied flow ($U = 0$). The validity of Eq. (3) is supported by the linear variation of V_{cx} with U in Fig. 3.

The experimental data of Figure 3 allow one to determine the values of the coefficients λ_s and λ_p; λ_s is first obtained by means of Eq. (4); its values in the oscillating and stationary regimes are plotted in Figure 4. In both cases, the experimental variation of λ_s with D/H is similar to that predicted by Ben Richou *et al.*[8,9] (also plotted on the figure). The difference between the experimental and predicted data is at most 15% and is likely due to the difference between the Reynolds numbers used by these authors, which are lower by a factor of 10 or more than in the present work; as shown by Hu[6] and Ben Richou,[9] the higher Reynolds number leads to a larger value of λ_s.

Note that the influence of the space between the ends of the rod and the lateral sides of the cell cannot account for this difference: the corresponding bypass flow would indeed instead reduce the measured value of λ_s (see Fig. 9 in Ref. 18). For $D/H = 0.48$, the transition from the stationary to the oscillation regime leads to a small increase ($\sim$15%) of λ_s. This variation reflects the complex interplay between the rolling motion of the cylinder and its displacement across the gap during the oscillations. The values in the two regimes are however remarkably similar.

The second factor λ_p is determined from the slope of the curves V_{cx} vs U in Fig. 3; from Eq. (3), this slope must indeed be equal to λ_p/λ_s. Again, the experimental values of λ_p are higher than the theoretical ones for the same reason as for λ_s (Fig. 4).

D. Characteristic velocity and Reynolds number of the phenomenon

From Eq. (1), the data points of Fig. 3 for a given cylinder and fluid all correspond to a same drag force $-mg$ so that

$$F_x = -mg = \lambda_p \mu \left[U - \frac{\lambda_s}{\lambda_p} V_{cx} \right]. \tag{5}$$

For a set of values of U and V_{cx}, the drag force can therefore be deduced from the value obtained for a stationary cylinder ($V_{cx} = 0$) by replacing U by the "effective" relative velocity

$$V_r = \left[U - \frac{\lambda_s}{\lambda_p} V_{cx} \right]. \tag{6}$$

V_r appears therefore as the logical characteristic velocity for characterizing the flow around the cylinder in all cases. The value of λ_s/λ_p varies slightly from one curve of Fig. 3 to another but, for all cases when oscillations are observed, one has $\lambda_s/\lambda_p = 0.8 \pm 0.03$. For simplicity, the value 0.8 is therefore applied in the following to the oscillatory regime (this choice has not a critical influence on the results); in particular, the Reynolds number is defined by

$$Re = \frac{\rho_f H V_r}{\mu} = \frac{\rho_f H |U - 0.8 V_{cx}|}{\mu}, \tag{7}$$

in which ρ_f and μ are the fluid density and viscosity. Let us point that, from Fig. 3 and the above discussion, V_r (and therefore Re) remains nearly constant for all experiments corresponding to a given fluid-cylinder pair and a given regime (oscillatory or stationary).

The choice of H as the characteristic length will be justified *a posteriori* by the analysis of the data in Sec. IV B. For $V_{cx} = 0$ (cylinder fixed on the average in a flow), Eq. (7) is equivalent to the definition of Re used by Semin *et al.*[17] For comparison of the present results with those of other authors, it must be taken into account that the definition $Re_D = \rho_f UD/\mu$ is often used instead of Re[8,12,13] for studying vortex emission behind fixed cylinders. In the case of a cylinder moving in a quiescent fluid ($U = 0$), Re is also replaced in Refs. 6 and 9 by $Re_D = \rho_f V_{cx} D/\mu$.

IV. OSCILLATORY REGIME

A. Amplitude of the transverse oscillations in the gap

Fig. 5 displays variations with time of the transverse coordinate y_c of the cylinder for different upward flow velocities U. As mentioned above, the corresponding diameter of the cylinder ($D = 1.45$ mm) is the lowest for which oscillations were observed. Moreover, their growth characteristics depends on U although the Reynolds number associated to the relative velocity V_r is approximately independent of U ($Re \simeq 49 \pm 1$). For $U = 0$, the cylinder is not well centered between the walls and it is difficult to perform reliable measurements. For $-6.3 \leq U \leq -2$ mm s^{-1}, the development of oscillations depends on the initial conditions. A stationary motion remains so while the cylinder keeps oscillating if it has been perturbed initially, for instance by increasing and decreasing $|U|$. For $U \leq -8.4$ mm s^{-1}, the oscillations appear spontaneously after a time decreasing from a few seconds for $U \simeq -10$ mm s^{-1} to a value too short to measure for $U \simeq -15$ mm s^{-1}. When the duration of the transient phase is long enough, this allow one to measure a meaningful value of V_{cx}, which is included as a no-oscillation data in Fig. 3. The oscillation amplitude $|A|$ in the stationary regime increases rapidly from a low value $|A| \sim 0.3$ mm right above the threshold ($U = -2.1$ mm s^{-1}) up to $|A| \simeq 1.3$ mm for $U \leq -4$ mm s^{-1}. This maximum value is close to the clearance between the cylinders and the cell walls ($H - D \simeq 1.55$mm): then, the cylinders come very close to the walls during their motion and may even touch them. This is confirmed by the clipping effect observed on the curve corresponding to $U = -12$ mm s^{-1} ($Re = 19$). Similar features are observed for the variation as a function of U of the maximum $|V_{cy}^0|$ of the transverse velocity dy_c/dt during an oscillation (this maximum is reached for $y_c \simeq 0$). This variation is plotted in Fig. 6 for different cylinders and for solutions $N1$ and $N2$. The velocity $|V_{cy}^0|$ can generally be considered as constant with U but decreases as the diameter of the cylinder increases ((○) symbols in Fig. 6). $|V_{cy}^0|$ also increases as the density of the cylinder and the

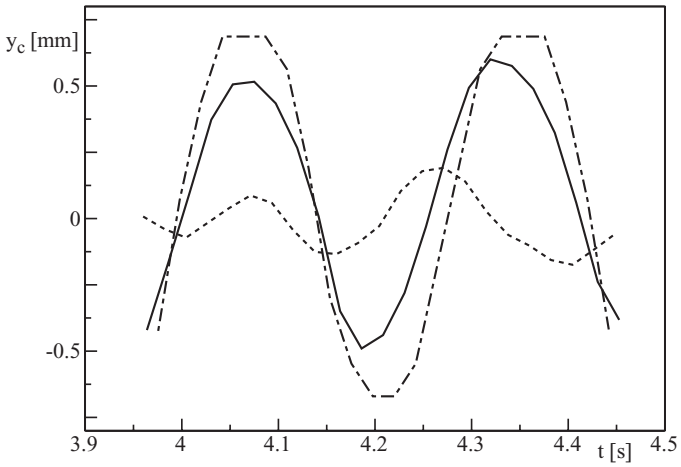

FIG. 5. (a) Variation of the transverse coordinate y_c of a PMMA cylinder ($D = 1.45$ mm) in the gap as a function of time for different mean velocities U of solution $N1$ (for better visibility, only a small part of the total recording time is shown). Dotted line: ($U = -2$ mm s^{-1}, $Re = 50$), solid line: ($U = -4$ mm s^{-1}, $Re = 49.5$), dashed-dotted line: ($U = -12$ mm s^{-1}, $Re = 48$).

viscosity of the fluid become larger ((▽) symbols in Fig. 6). The stronger dispersion of the values for the carbon cylinder results both from the larger drift velocity, which reduces the measurement time and from the higher value of $|V_{cy}|$, which makes the measurements less precise at the limited frame rate available.

B. Frequency of the oscillations

The comparison of the continuous and dashed-dotted curves in Fig. 5 suggests that (again except close to the threshold), the frequency f of the oscillation depends weakly on the flow velocity U. More quantitatively, the frequency values obtained as described in Sec. III A for four different cylinder diameters and for the two solutions $N1$ and $N2$ are plotted as a function of U in Figure 7. For all curves, the typical relative deviation of f from its mean value as U varies is indeed less than $\pm 5\%$. It should be noted that, for $D = 2.1$ mm, a fluttering motion superimposed onto the transverse oscillation is observed: in view of the similar value of f compared to other ratios D/H, this does not appear to influence significantly the instability.

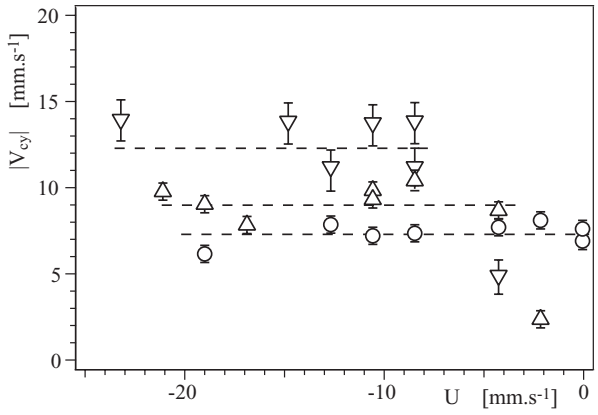

FIG. 6. Maximum velocity $|V_{cy}|^0$ of the transverse oscillations inside the gap as a function of the mean flow velocity U. (△), (○): PMMA cylinders of respective diameters $D = 1.45$ and $D = 1.63$ mm in solution $N1$. (▽): carbon cylinder in solution $N2$ ($D = 1.45$ mm).

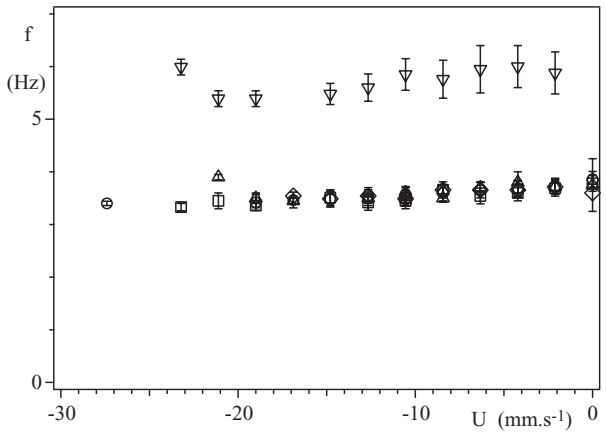

FIG. 7. Variation of the oscillation frequency as a function of *Re* for different cylinders and Natrosol concentrations. Solution *N*1 and PMMA cylinders of diameters $D = 1.45$ mm (△); $D = 1.63$ mm (○); $D = 1.77$ mm (□); $D = 2.1$ mm (◊); solution *N*2 and carbon cylinders of diameter $D = 1.45$ mm (▽).

This weak dependence on U of both the amplitude and the frequency of the oscillations (Figs. 6 and 7) confirms that V_r (constant for each fluid-cylinder pair), and not U or V_{cx} separately, is the relevant characteristic velocity of the problem. Another evidence is that, still for a given fluid-cylinder pair, either oscillations occur for all values of U or the motion remain stationary. At a given *Re* value, one is therefore either above or below the threshold Re_c at all flow velocities U: then, in contrast with tethered cylinders,[17] Re_c cannot be determined by varying U.

The pair $D = 1.45$ mm - fluid *N*1 corresponds likely to the vicinity of the threshold: both the stationary and the oscillating regimes are observed with, frequently, a transition during the motion. Oscillations are more easily observed at U values such that V_{cx} is low because the cylinder remains longer within the field of view and the instability has more time to develop.

A second important feature is that all frequency variation curves corresponding to the same solution *N*1 but to different diameters D almost coincide over most of the range of variation of U: this supports the assumption that H (and not D) is the relevant characteristic length of the problem.

Finally, the frequency f increases by 70% when solution *N*1 is replaced by *N*2 with twice its viscosity. However, in order to observe these oscillations, the PMMA cylinder must be replaced by a carbon one of same diameter $D = 1.45$ mm but higher density (1.54 instead of 1.2 g cm^{-3}): due to this larger density, the relative velocity V_r is higher, as can be seen in Figure 3. The increase of f may therefore result from that of ν and/or of V_r; Ref. 17 suggests, in addition, that the increase of the weight of the cylinder may directly reduce f but only by a few % so that this last effect is neglected.

As a test of the dependence of f on ν, we have plotted in Fig. 8 the dimensionless parameter $fH^2/\nu = f\tau_\nu$ as a function of the Reynolds number *Re* (τ_ν is the characteristic viscous diffusion time over the distance H). As could be expected from Fig. 7, the product $f\tau_\nu$ is nearly constant for all PMMA cylinders with

$$f = (29 \pm 2)\,\frac{\nu}{H^2}. \tag{8}$$

For the more viscous solution *N*2 and the denser carbon cylinder, the normalized values (▽ symbols) are closer to the above ones than in the plot of Fig. 7 (they are lower by 20% with $f\tau_\nu \simeq 23$).

It must be noted that, for a given cylinder-fluid pair, nearly all data points of Fig. 8 correspond to a very small range of *Re* values (since *Re* is nearly independent of U). Therefore, in contrast with studies using fixed or tethered cylinders, the dependence of f on *Re* reflects the variation from one fluid-cylinder pair to another and not a variation with *Re* for a single pair.

In order to compare these results to those reported for related configurations and to test the influence of V_r, we also plotted in the inset of Fig. 8, together with data from Ref. 17, the variation

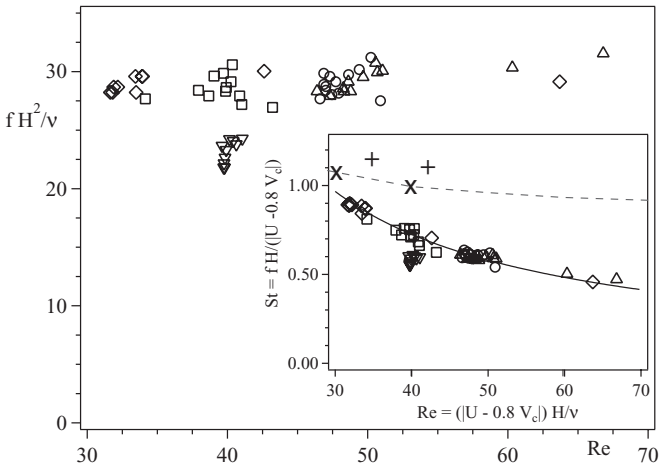

FIG. 8. Variation of the normalized frequency fH^2/ν as a function of Re for different cylinder diameters and Natrosol concentrations. Inset: variation of the Strouhal number $St = fH/|V_r| = fH/|U - 0.8V_{cx}|$ as a function of the Reynolds number Re for the same experiments. Continuous line: variation as $St = 30/Re$; dotted line and ($\times$) symbols: results of numerical simulations for a tethered cylinder with $D/H = 0.67$ from Ref. 17; (+) symbols: experimental data from the same reference. In both graphs, the meaning of the other symbols is the same as in Fig. 7.

with Re of the Strouhal number

$$St = \frac{f.H}{|U - 0.8\,V_{cx}|} = \frac{f.H}{|V_r|}. \tag{9}$$

For data obtained with solution $N1$ and the PMMA cylinder, the nearly constant value of fH^2/ν leads to a good collapse of the points on a common decreasing trend: $St \propto Re^{-1}$ (reflecting the relation $St = f\tau_\nu\, Re^{-1}$). This plot also brings the data points for solution $N2$ and the carbon cylinder closer to the global trend, although with values 15% lower.

Overall, the different dimensionless plots of Fig. 8 do not indicate therefore a dominant dependence of f on either ν or V_r: further experiments and numerical simulations in which one of these parameters will be controlled separately are therefore needed to solve this issue.

The closest comparison basis for the variation of St with Re discussed above is provided by numerical simulations and experiments reported for a tethered cylinder in a similar flow geometry[17] (dotted line in the inset of Fig. 8). These data correspond to the single blockage ratio $D/H = 0.67$ and to several values of Re; for the present data, instead, Re is practically constant for a given value of D/H. New simulations and/or experiments with tethered cylinders (possibly free to rotate) will be needed to extend the comparison to other values of D/H. Here, the comparison can only be performed at the values of Re corresponding to blockage ratios as close as possible to 0.67: the two nearest ones are $D/H = 0.7$ ($D = 2.1$ mm) and $D/H = 0.59$ ($D = 1.77$ mm), which correspond, respectively, to $Re \simeq 32$ and $Re \simeq 40$.

The data from Ref. 17 for which Re is close to these values are shown by the symbols ($\times$) for numerical simulations and (+) for experiments. For $D/H = 0.7$ which is closest to the target value 0.67, St is, respectively, 20% and 30% lower for the experiments with the free cylinder than for the simulations and the experiments using the tethered one. The difference is larger (30% and 45%) for $D/H = 0.59$, which is farther from the target value 0.67. In spite of this difference, the values of the Strouhal number are similar enough so that one may assume that the two oscillation phenomena correspond to a same global mechanism.

A possible origin of the difference between these values of the frequency is the influence of the additional degrees of freedom of the cylinder in the present work, i.e., rotation and vertical motion. As will be seen in Sec. IV C, the tangential velocity associated to the rotation is of the same order as the mean velocity $|U|$: it may therefore influence significantly the characteristics and the onset of the oscillations. The very strong coupling between the oscillations of the cylinder and its global motion is indeed shown for $D/H = 1.45$ by the strong reduction of the velocity V_{cx} between the

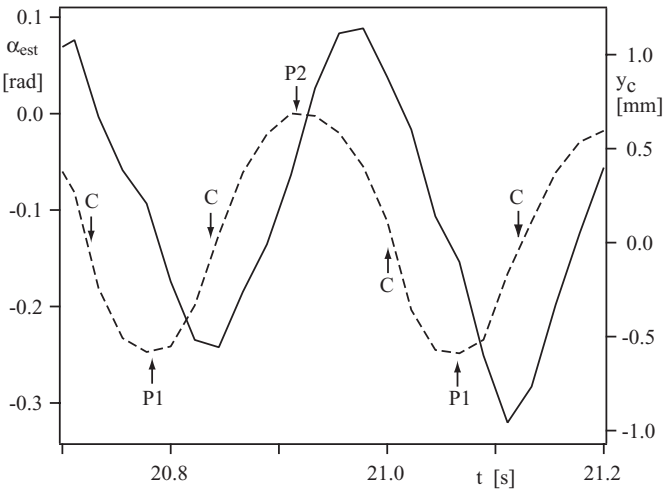

FIG. 9. Oscillations of a PMMA cylinder $D = 1.45$ mm in solution $N1$ flowing at $U = -12.7$ mm s-1 ($Re = 48.5$). Solid line: estimated roll angle α_{est}; dashed line: transverse coordinate y_c. The origin of the α axis is arbitrary.

stationary and the oscillation regimes (Fig. 3). Further tests such as numerical simulations in which the degrees of freedom can be released independently are however needed to test their respective influence. Although small, the residual clearance between the ends of the cylinder and the sides of the cell may also introduce frequency variations by creating a by-pass for the fluid at the ends of the cylinder.[18]

C. Time variation of the roll angle α

The variations with time of the both the estimated roll angle α_{est} and the transverse coordinate y_c are plotted in Fig. 9. Both parameters oscillate periodically at the same frequency f. The roughly triangular shape of the variation of α_{est} suggests a sharp change of the direction of rotation shortly after the cylinder reaches its minimal distance ($\simeq 200\,\mu$m) to a wall. A strong interaction with the latter may account for this effect but it may also be influenced by the nonlinear relation between the estimated angle and the actual value of α.

As the cylinder moves towards one of the walls, it rotates always in the direction opposite to the local vorticity corresponding to the mean flow (see Fig. 1); the rotation changes direction while it moves away so that it is again opposite to the local vorticity when it reaches the other wall. The corresponding absolute tangential velocity $|\dot{\alpha}|D/2$ of the surface of the cylinder at that time is close to 9 mm s^{-1}. This latter value is of the same order of magnitude as the absolute flow velocity $|U|$: as mentioned in the above section, this rolling motion may therefore influence significantly the oscillation process.

D. Variation with time of the vertical velocity

Figure 10 displays the vertical and transverse coordinates x_c and y_c of the cylinder axis as a function of time during 4 oscillations. In this oscillating regime, the vertical coordinate x_c of the cylinder still follows a global linear trend with time but the velocity $V_{cx} = (dx_c/dt)$ displays periodic oscillating deviations from its mean value$(dx_c/dt)_0$ clearly visible in the inset of Figure 10. These latter variations imply similar ones for the drag while the cylinder moves across the gap.

The variation of $(dx_c/dt) - (dx_c/dt)_0$ displays two minima for each period of the oscillation, each one when the cylinder is near one of the walls ($(P1)$ or $(P2)$): this corresponds to a second harmonic of the frequency of the transverse oscillation. Such a frequency component was also observed (and was in that case dominant) in the variation of x_c in Fig. 2(c). In this latter experiment, the time average of the velocity (dx_c/dt) is zero, in contrast to the present case. This frequency-doubling effect results

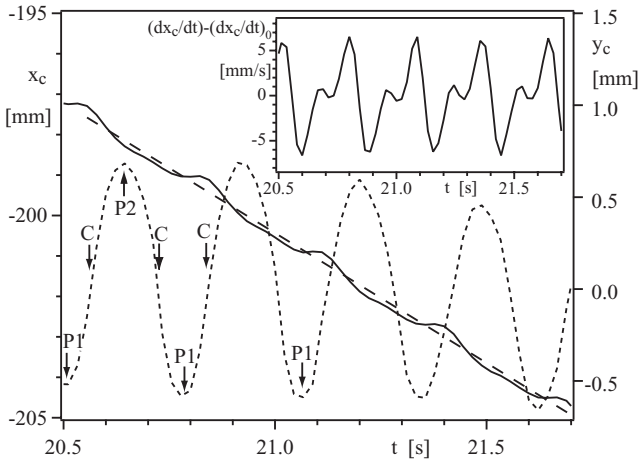

FIG. 10. Time variation of the vertical coordinate x_c (solid line) and of the transverse coordinate y_c (dashed line) as a function of time for the same experiment as in Fig. 9. Inset: time variation of the deviation $(dx_c/dt) - (dx_c/dt)_0$ of the vertical velocity from its mean value $(dx_c/dt)_0$ deduced from a linear regression over $x_c(t)$.

from the symmetry of the problem with respect to the mid plane of the cell. Let us assume first that no rotation is present: moving the cylinder towards either of the walls leads to distortions of the flow field and the resulting x component of the force is the same for the two walls while the y components are opposite. If, in addition, there was a continuous rotation of the cylinder, this symmetry would be broken: it is however recovered in the present oscillating regime because the rotation changes sign at each half period and the relative velocity of the cylinder and the nearest wall remains the same. Globally, therefore, the periodicity of the vertical force components corresponds to half the period of the transverse oscillations.

In the inset of Fig. 10, one of the minima corresponding to each period is much shallower than the other. This may imply that the transverse oscillation between the two walls is not symmetrical with respect to the mid plane $y_c = 0$ and/or that the motion of the cylinder is not completely two dimensional.

V. DISCUSSION AND CONCLUSION

The experiments reported in this work have demonstrated that cylinders free to rotate and translate in a vertical confined Hele Shaw cell may display transverse oscillations of large amplitude: these oscillations were only observed for a confinement parameter $D/H \geq 0.48$; at this lower value, and for fluid N1, spontaneous transitions towards the oscillatory regime are observed, particularly at low cylinder velocities V_{cx}. Actually, the key characteristic velocity of the oscillation process is not the flow velocity U of the fluid but the effective relative velocity $V_r = U - 0.8V_{cx}$ (or the corresponding Reynolds number $Re = |V_r|H/\nu$): the factor 0.8 corresponds to the slope of the experimental variation of V_{cx} with U. The latter variation reflects the balance between the effective weight of the cylinder and the viscous friction: as a result of this definition, V_r and Re remain nearly constant for a given cylinder-fluid pair when U varies. For instance, the frequency of the oscillations and the corresponding transverse velocity are nearly the same for a cylinder sedimenting in a static fluid ($U = 0$) or kept at a constant average height x_c by an upward flow. More generally, the frequency, the amplitude and the occurrence of the oscillations as well as the relative velocity V_r (and Re) do not depend on U for a given fluid-cylinder pair: as a result, and in contrast to tethered cylinders, the threshold Reynolds number for the onset of the oscillations cannot be determined by varying U for a given cylinder since Re remains nearly constant.

In this work, oscillations have been observed down to Reynolds numbers Re as low as 30, which is of the same order of magnitude as for tethered cylinders.[17] Compared to them, the present phenomenon involves additional kinetic energy contributions associated to new degrees of freedom

(rotation, vertical motion, tilt angle with respect to the horizontal). For moderate confinements ($0.48 \leq D/H \lesssim 0.6$), the phenomenon remains bidimensional. This agrees with observations of an increase of the critical Re value for the onset of $3D$ instabilities for confined cylinders.[19] In this $2D$ regime, the motion of the cylinder combines transverse and rotational oscillations at the fundamental frequency f and vertical oscillations generally superimposed onto a global vertical drift. The latter have a component at the frequency $2f$ accounted for by the symmetry of the system. At higher values of D/H such as 0.7, a fluttering $3D$ motion of the cylinder appears with oscillations of its angle with respect to the horizontal and of its lateral position (coordinate z) at a lower frequency. This is likely due to the strong blockage of the flow at large D/H values by the cylinder, which occupies 90% of the cell width.

On the one hand, for a fixed cylinder density ρ_s and given fluid density and viscosity, the frequency f of the oscillations is not only independent of the velocity U but, also, of the confinement D/H. On the other hand, increasing at the same time ν and ρ_s (and, as a result, the velocity V_r) led to 70% larger f values. The constant value of f for a varying D/H ratio is a puzzling feature. However, while the relative velocity V_r is practically constant with U, it depends on D/H (see Fig. 3): it is therefore possible that variations of f due to those of V_r and D/H compensate each other. Further studies with a separate investigation of the influence of these variables will be necessary.

The scaling laws of the problem have been searched for by replotting the frequencies in a dimensionless form ($St = fH/\nu$ and $f\tau_\nu = fH^2/\nu$) as a function of the Reynolds number Re. The Strouhal number is classically applied to inertial flow induced oscillations while fH^2/ν is based on the viscous diffusion time τ_ν and is suitable for viscous processes; the oscillation might indeed result from a phase shift due to viscous diffusion between the motion of the cylinder and the corresponding variations of the flow and pressure fields.

For the PMMA cylinders and the $N1$ solution, the constant value of f leads to a variation of the Strouhal number $St \propto 1/Re$ and to a nearly constant product $f\tau_\nu \simeq 29$. For the more viscous solution $N2$ and the denser cylinder, the two types of adimensionalization reduce to $15\% - 20\%$ the relative difference (compared to Fig. 7) with the global trends with, this time, lower values than in the latter. There is therefore no conclusive advantage of one type of adimensionalization compared to the other.

Globally, these results contrast with those reported for many oscillatory instabilities such as vortex shedding:[12,15] in this case, the Strouhal number increases first with the Reynolds number above the threshold before becoming constant. However, such variations are measured on a single fluid-cylinder pair with varying flow velocities; here, instead, the plots of Fig. 8 combine results corresponding to different ratios D/H, each of them corresponding to a very narrow range of Re values. The influence of the different control parameters such as D/H, ν, and ρ_s will therefore have to be studied separately in future work.

The properties of the frequency f have a direct relation to the variation of the transverse velocity $|V_{cy}|$ in the gap at large oscillation amplitudes. Assuming a constant absolute value of $|V_{cy}|$ during these oscillations and a peak to peak amplitude $(D - H)$ of the latter leads to the estimation

$$|V_{cy}| \simeq 2f(H - D). \tag{10}$$

Like f, the velocity $|V_{cy}|$ should then be independent of the mean flow velocity U (for a given fluid-cylinder pair) as indeed observed in Fig. 6 for $|U| \geq 5$. Equation (10) also predicts that $|V_{cy}|$ increases with the frequency f and decreases as the diameter D increases, also in agreement with the data of Fig. 6.

For comparison purposes, the phenomenon closest to the present one is likely the oscillation of tethered cylinders in the same flow geometry[17] although, as discussed above, the additional degrees of freedom may introduce differences. For $Re \simeq 32$ and $D/H = 0.7$, the Strouhal number in the present experiments is 20% lower than for numerical simulations. A part of this difference is likely accounted for by the additional degrees of freedom. It will be important to confirm and explain these results, in particular by numerical simulations at different D/H values in which the different degrees of freedom may be introduced independently. Another issue is the influence of these degrees of freedom on the threshold value of Re, which may be determined numerically, for instance, by varying the acceleration of gravity to control Re.

Another question is the possible relation between the present oscillations and those resulting from vortex shedding. For fixed confined cylinders,[12,20] the discussion of Sec. III A shows that vortex shedding takes place at Reynolds numbers much larger than those for which the present oscillations occur: for $D/H = 0.7$ and using the present definition, the values of Re_c are, respectively, 110 and less than 30. A similar increase of Re_c due to confinement has also been reported for a lower ratio $D/H = 1/3$.[21] Also, the Strouhal number St often increases with Re above the threshold for vortex shedding[12,20] while it decreases instead with Re for the type of instabilities studied here (dotted line in the inset of Fig. 8).

For a moving cylinder, Hu[6] reports oscillations due to vortex shedding for a cylinder sedimenting between parallel plates ($D/H = 0.25$) and close to one of them at $Re = 320$, i.e., still at a value of Re much larger than 100. For an infinite fluid, Namkoong *et al.*[22] report a slightly larger threshold Re_{cD} and a 10% lower Strouhal number St_D for vortex emission behind a sedimenting cylinder than behind a fixed one (both Re and St are based in this case on the diameter D). Finally, Ref. 17 reports oscillations due to vortex shedding only for $Re \gtrsim 110$ for tethered cylinders in a geometry close to the present one: moreover, for high cylinder densities, confinement induced oscillations (likely similar to the present ones) and vortex induced ones take place in distinct ranges of Re values and the latter are of significantly lower amplitude. On the other hand, reduced critical Re values have been reported when additional degrees of freedom are introduced for 2D bodies rising or falling in a fluid:[23,24] however, this occurs in the case of non-circular cross sections.

Globally, while the above results do not completely rule out the occurrence of vortex shedding in the present work, they suggest that the mechanism of the oscillations is different and likely more dependent on the viscosity: its influence will have to be investigated further in future work. Actually, the present results and those of Ref. 17 suggest that the present instability occurs only if the cylinder can oscillate while vortex shedding is observed even for fixed cylinders and, for free cylinders, generates forced oscillations of smaller amplitude.

Finally, for large D/H ratios, the clearance between the ends of the cylinders and the sides of the cell may have an important influence. For cylinders of length L_c significantly lower than W, the bypass effect may influence the process and/or induce a fluttering motion. It will be interesting to compare this latter phenomenon to motions involving a coupling between the vertical motion of objects and lateral oscillations: these are encountered in such problems as the fall of leaves or paper sheets,[25,26] of disks[27] or the rise of bubbles in a liquid.[28]

ACKNOWLEDGMENTS

We thank R. Pidoux, L. Auffay, and A. Aubertin for realizing and developing the experimental set up and B. Semin for his careful reading of the manuscript and his useful comments. We acknowledge the RTRA Triangle de la Physique and the LIA PMF-FMF (Franco-Argentinian International Associated Laboratory in the Physics and Mechanics of Fluids). The work of one of us (V.D.) was supported by a Bernardo Houssay grant allocated by the Argentinean and French ministries of research.

[1] R. Rusconi, S. Lecuyer, L. Guglielmini, and H. Stone, "Laminar flow around corners triggers the formation of biofilm streamers," J. R. Soc., Interface **7**, 1293–1299 (2010).
[2] N. Autrusson, L. Guglielmini, S. Lecuyer, R. Rusconi, and H. A. Stone , "The shape of an elastic filament in a two-dimensional corner flow," Phys. Fluids **23**, 063602 (2011).
[3] A. S. Dvinsky and A. S. Popel, "Motion of a rigid cylinder between parallel plates in Stokes flow. Part 1: Motion in a quiescent fluid and sedimentation," Comput. Fluids **15**, 391–404 (1987).
[4] A. S. Dvinsky and A. S. Popel, "Motion of a rigid cylinder between parallel plates in Stokes flow. Part 2: Poiseuille and Couette flow," Comput. Fluids **15**, 405–419 (1987).
[5] E. Eklund and A. Jernqvist, "The motion of a neutrally buoyant circular cylinder in bounded shear flows," Chem. Eng. Sci. **49**, 3765–3772 (1994).
[6] H. H. Hu, "Motion of a circular cylinder in a viscous liquid between parallel plates," Theor. Comput. Fluid Dyn. **7**, 441–455 (1995).
[7] H. Faxén, "Forces exerted on a rigid cylinder in a viscous fluid between two parallel fixed planes," Proc. R. Swed. Acad. Eng. Sci. **187**, 1–13 (1946).
[8] A. B. Richou, A. Ambari, and J. K. Naciri, "Drag force on a circular cylinder midway between two parallel plates at very low Reynolds numbers. Part 1: Poiseuille flow (numerical)," Chem. Eng. Sci. **59**, 3215–3222 (2004).

[9] A. B. Richou, A. Ambari, M. Lebey, and J. K. Naciri, "Drag force on a cylinder midway between two parallel plates at $Re \ll 1$. Part 2: Moving uniformly (numerical and experimental)," Chem. Eng. Sci. **60**, 2535–2543 (2005).
[10] S. Champmartin, A. Ambari, and N. Roussel, "Flow around a confined rotating cylinder at small Reynolds number," Phys. Fluids **19**, 103101 (2007).
[11] H. Juarez, L. R. Scott, R. Metcalfe, and B. Bagheri, "Direct simulation of freely rotating cylinders in viscous flows by high-order finite element methods," Comput. Fluids **29**, 547–582 (2000).
[12] M. Sahin and R. G. Owens, "A numerical investigation of wall effects up to high blockage ratios on two-dimensional flow past a confined circular cylinder," Phys. Fluids **16**, 1305–1320 (2004).
[13] L. Zovatto and G. Pedrizetti, "Flow about a circular cylinder between parallel walls," J. Fluid Mech. **440**, 1–25 (2001).
[14] D. Shiels, A. Leonard, and A. Roshko, "Flow-induced vibration of a circular cylinder at limiting structural parameters," J. Fluids Struct. **15**, 3–21 (2001).
[15] C. H. K. Williamson and R. Govardhan, "A brief review of recent results in vortex-induced vibrations," J. Wind Eng. Ind. Aerodyn. **96**, 713–735 (2008).
[16] M. P. Païdoussis, S. J. Price, and E. de Langre, *Fluid-Structure Interactions—Cross-Flow-Induced Instabilities* (Cambridge University Press, Cambridge, 2011).
[17] B. Semin, A. Decoene, J. P. Hulin, M. L. M. Francois, and H. Auradou, "New oscillatory instability of a confined cylinder in a flow below the vortex shedding threshold," J. Fluid Mech. **690**, 345–365 (2012).
[18] B. Semin, J.-P. Hulin, and H. Auradou, "Influence of flow confinement on the drag force on a static cylinder," Phys. Fluids **21**, 103604 (2009).
[19] S. Camarri and F. Giannetti, "Effect of confinement on three-dimensional stability in the wake of a circular cylinder," J. Fluid Mech. **642**, 477–487 (2010).
[20] C. H. K. Williamson, "Vortex dynamics in the cylinder wake," Annu. Rev. Fluid Mech. **28**, 477–539 (1996).
[21] F. Rehimi, F. Alouia, S. B. Nasrallahb, L. Doublieza, and J. Legrand, "Experimental investigation of a confined flow downstream of a circular cylinder centred between two parallel walls," J. Fluid. Struct. **24**, 855–882 (2008).
[22] K. Namkoong, J. Y. Yoo, and H. G. Choi, "Numerical analysis of two-dimensional motion of a freely falling circular cylinder in an infinite fluid," J. Fluid Mech. **604**, 33–53 (2008).
[23] P. Ern, F. Risso, D. Fabre, and J. Magnaudet, "Wake-induced oscillatory paths of bodies freely rising or falling in fluids," Ann. Rev. Fluid Mech. **44**, 97–121 (2012).
[24] P. Assemat, D. Fabre, and J. Magnaudet, "The onset of unsteadiness of two-dimensional bodies falling or rising freely in a viscous fluid: A linear study," J. Fluid Mech. **690**, 173–202 (2012).
[25] Y. Tanabe and K. Kaneko, "Behavior of a falling paper," Phys. Rev. Lett. **73**, 1372–1375 (1994).
[26] A. Belmonte, H. Eisenberg, and E. Moses, "From flutter to tumble, inertial drag and Froude similarity in falling paper," Phys. Rev. Lett. **81**, 345–348 (1998).
[27] P. Ern, P. C. Fernandes, F. Risso, and J. Magnaudet, "Evolution of wake structure and wake-induced loads along the path of freely rising axisymmetric bodies," Phys. Fluids **19**, 113302 (2007).
[28] J. Magnaudet and I. Eames, "The motion of high-Reynolds-number bubbles in inhomogeneous flows," Annu. Rev. Fluid Mech. **32**, 659–708 (2000).